Behavioral/Systems/Cognitive

Exploiting Development to Evaluate Auditory Encoding of Amplitude Modulation

Merri J. Rosen,[1] Malcolm N. Semple,[2,4] and Dan H. Sanes[2,3]

[1]Department of Anatomy and Neurobiology, Northeastern Ohio Universities College of Medicine, Rootstown, Ohio 44272, and [2]Center for Neural Science and Departments of [3]Biology and [4]Psychology, New York University, New York, New York 10003

During development, detection for many percepts matures gradually. This provides a natural system in which to investigate the neural mechanisms underlying performance differences: those aspects of neural activity that mature in conjunction with behavioral performance are more likely to subserve detection. In principle, the limitations on performance could be attributable to either immature sensory encoding mechanisms or an immature decoding of an already-mature sensory representation. To evaluate these alternatives in awake gerbil auditory cortex, we measured neural detection of sinusoidally amplitude-modulated (sAM) stimuli, for which behavioral detection thresholds display a prolonged maturation. A comparison of single-unit responses in juveniles and adults revealed that encoding of static tones was adult like in juveniles, but responses to sAM depth were immature. Since perceptual performance may reflect the activity of an animal's most sensitive neurons, we analyzed the d prime curves of single neurons and found an equivalent percentage with highly sensitive thresholds in juvenile and adult animals. In contrast, perceptual performance may reflect the pooling of information from neurons with a range of sensitivities. We evaluated a pooling model that assumes convergence of a population of inputs at a downstream target neuron and found poorer sAM detection thresholds for juveniles. Thus, if sAM detection is based on the most sensitive neurons, then immature behavioral performance is best explained by an immature decoding mechanism. However, if sAM detection is based on a population response, then immature detection thresholds are more likely caused by an inadequate sensory representation.

Introduction

The relationship between perception and neural encoding is well studied in adult animals, but seldom during development when perceptual abilities are most dynamic. In humans, auditory perceptual skills mature well into the teenage years. For example, detection thresholds for sinusoidally amplitude-modulated (sAM) sounds reach maturity during the first decade (Hall and Grose, 1994; Banai et al., 2007), and a similar trajectory is reported for gerbils: the average initial sAM detection threshold for adults is ~31% modulation depth (MD) compared with ~45% for juveniles at postnatal day 30 (P30) to P38 (Sarro and Sanes, 2010). This developmental difference is not correlated with behavioral measures commonly associated with attention (e.g., false alarm rate), suggesting that the sensory encoding mechanisms could display a similar developmental trajectory. The goal of this study was to exploit developmental changes to evaluate candidate sAM encoding mechanisms. Thus, we obtained auditory cortex (ACx) spiking responses to sAM stimuli in awake juvenile and adult gerbils and applied neurometric analyses to determine which aspects of neural maturation parallel the developmental improvement in perception.

One reason to focus on sAM processing is its relevance to animal communication (Rosen, 1992; Shannon et al., 1995; Singh and Theunissen, 2003). For example, MDs (i.e., the magnitude of periodic increase and decrease in sound amplitude) as low as 10% are found in speech fricatives (Pincas and Jackson, 2006), and MD variations influence comprehension (Krause and Braida, 2004). Although behavioral sAM thresholds are quite low, neural responses are typically evoked at 100% MD (Zwicker, 1952; Viemeister, 1979; Salvi et al., 1982; Kohlrausch et al., 2000; Kelly et al., 2006). Whereas neural responses to shallow MDs have been characterized recently in adults (Middlebrooks, 2008; Malone et al., 2010), we have a poor understanding of their development.

We focused our analysis on ACx because it integrates brainstem and thalamic inputs and serves as the primary sensory representation to decoding centers (Budinger et al., 2000, 2006; Kaas and Hackett, 2000). Furthermore, temporal discrimination is accompanied by activation of left ACx and is impaired by ACx ablation or inactivation (Elliott and Trahiotis, 1972; Ohl et al., 1999). Additionally, although many studies have characterized the maturation of ACx processing (Eggermont, 1991; Bonham et al., 2004; Pienkowski and Harrison, 2005; Razak and Fuzessery, 2007b; Brown and Harrison, 2010), all used anesthetized preparations, yielding data that might differ significantly from awake recordings, especially in ACx (Gaese and Ostwald, 2001; Wang et al., 2005).

To evaluate neural encoding, we transformed the sAM-evoked spike trains into a form that could be compared directly

Received June 23, 2010; revised Aug. 11, 2010; accepted Sept. 14, 2010.

This work was supported by the National Institute on Deafness and Other Communication Disorders Grants DC009165 (M.J.R) and DC009237 (D.H.S.), the National Organization of Hearing Research (M.J.R.), and the New York University Research Challenge Fund (D.H.S.). We thank Tony Movshon, Keith Purpura, Robert Froemke, Brian Malone, Anne Marie Oswald, and Sharad Shanbhag for many helpful ideas, discussions, and/or comments on this manuscript.

Correspondence should be addressed to Merri J. Rosen, Department of Anatomy and Neurobiology, Northeastern Ohio Universities College of Medicine, 4209 State Route 44, P.O. Box 95, Rootstown, OH 44272. E-mail: mrosen@neoucom.edu.

DOI:10.1523/JNEUROSCI.3340-10.2010

 0270-6474/10/3015509-12$15.00/0

with measures of behavioral performance in juvenile and adult gerbils. Well tuned sensory neurons are typically evaluated with optimal stimuli to determine whether their responses correlate with perception. This approach does not consider those cells that are active but not well tuned. Population coding schemes posit that all active neurons contribute to perception, whereas the lower envelope principle posits that animals can rely on their most sensitive neurons and that less sensitive neurons will not interfere with the percept (Parker and Newsome, 1998). Our results show that the best ACx neurons at each age are equivalently sensitive, indicating that the lower envelope principle is not sufficient to explain behavioral differences. In contrast, a population analysis that sums tuned and untuned neurons is sufficient to explain the maturation of sAM detection thresholds observed in behaving gerbils.

Materials and Methods

All procedures relating to the maintenance and use of animals in this study were approved by the University Animal Welfare Committee at New York University. A total of 13 adult (P60–P73, six males and seven females) and 12 juvenile (P29–P40, seven males and five females) Mongolian gerbils (*Meriones unguiculatus*) were used in this study.

Surgical preparation and chronic recordings

Gerbils were premedicated with ketoprophen (1.5 mg/kg, i.n.) and dexamethasone (0.35 mg/kg, i.p.) and hydrated with normosol (1.5 ml, s.c.). The animals were anesthetized with isoflurane, maintained by monitoring withdrawal reflexes and respiration rate. Animals were held in a stereotaxic apparatus. Several (six to eight) small bone screws were attached around the perimeter of the skull. A small headpost was positioned along the midline and secured with dental acrylic. A silver ground wire was secured in a small hole drilled into the posterior contralateral skull. A craniotomy was made over the left temporal cortex caudal to the bregma suture using stereotaxic coordinates (Thomas et al., 1993), and the dura was left intact. A thin well of dental acrylic was built along the perimeter of the craniotomy, and the enclosure was covered with silicone oil to maintain moisture and prevent surface edema. The craniotomized area was covered with a disposable cap of silicone elastomer (Sammons Preston Rolyan). The entire skull was covered with dental acrylic to form a headcap.

Animals were placed in a soundproof chamber (Industrial Acoustics Company), and the head was stabilized using the headpost. During chronic recording sessions, animals stood comfortably on a platform and were free to move their limbs while the head position remained fixed. If an animal exhibited heightened anxiety or restlessness, medetomidine (a relaxant that acts on 2-adrenoceptors) was administered intranasally at the beginning of the recording session at a dosage of one to three drops (0.1–0.3 mg/kg) and supplemented as necessary. Gerbils trained to detect amplitude modulation in our laboratory are able to perform the task after medetomidine administration (D. H. Sanes, unpublished observations). An additional analysis showed that key neural response properties (firing rate, minimum first-spike latency, and phase-locking cutoff frequency for sAM tones) remained stable with time elapsed after medetomidine administration (47–200 min) (Ter-Mikaelian et al., 2007). Because medetomidine did not produce an observable effect on neuronal activity, the results for cells recorded with and without medetomidine are presented together.

Electophysiological recordings

The silicone elastomer cap was removed at the beginning of each session, and a fresh cap was applied at the end. The dura was covered with saline during recording to maintain moisture. Platinum-plated tungsten electrodes (1.5–2.5 MΩ; MicroProbe) were advanced ventrally through the craniotomy with an electrode tip angle of 14° lateral to vertical to isolate neurons in primary ACx. Single-unit recording procedures were identical to those described previously (Ter-Mikaelian et al., 2007). The proportion of recorded cells for the two age groups and their corresponding best frequencies are shown in Figure 1.

Acoustic stimulation

The system used for stimulus generation and sound delivery (MALab; Kaiser Instruments) as well as the calibration procedure have been described previously (Malone and Semple, 2001). Calibrated acoustic stimuli were presented to each ear through an electrostatic speaker coupled to a custom-made ear insert. All stimuli were presented monaurally to the right ear except in cases in which a monaural stimulus failed to elicit reliable responses, in which case a binaural stimulus was used. Sound pressure level (SPL) is expressed relative to 20 μPa.

Each neuron was assessed with a battery of stimulus protocols designed to determine its response properties for static and modulated sounds. Typically, the approximate frequency range over which the neuron was responsive was obtained with an iso-intensity function at 10–30 dB above threshold (threshold criteria are described below). This was followed by a rate-level function (RLF) at the estimated best frequency (BF). The RLF was measured at increments of 5 dB SPL, using 200-ms-duration tone pips delivered at the BF of the unit. The pips were shaped with a 5 ms cosine-ramped rise/fall time and presented for at least 10 trials, with a 1 s intertrial interval.

sAM tones (2 s duration with 10 ms rise/fall) were presented at BF and at the SPL that produced the strongest response that was synchronized to the stimulus envelope (often the same as the best SPL for tone stimulation). Modulation transfer functions (MTFs) were obtained by presenting 5 or 10 trials of multiple modulation frequencies at 100% MD with an intertrial interval of 1 s. Modulation frequencies were typically 0.5, 1, 2, 5, 10, 20, 50, and 100 Hz. An unmodulated tone at the same frequency and SPL and of the same duration as the sAM tones was included in the stimulus sequence as a control. For a subset of cells, MTFs were instead obtained using two trials of 10 s sAM tones with a 10 ms rise time and an intertrial interval of 2 s. The best modulation frequency (BMF) was determined from the MTF as the modulation frequency eliciting the highest response strength (i.e., the product of firing rate and vector strength). Additional functions were measured at BMF, since by eliciting the strongest sAM-evoked response it provided the greatest number of spikes for analysis. Modulation depth functions (MDFs) were obtained by presenting 10 trials of multiple MDs at BF and BMF with an intertrial interval of 1 s. The following MDs were typically presented to each ACx neuron: 5, 10, 20, 50, 70, 80, and 100% MD.

Data analysis

RLFs and sAM responses. Spike times were stored and viewed as raster plots or peristimulus time histograms (PSTHs). Minimum first-spike latency was determined at BF and at the SPL that produced the earliest response by selecting the first peak in the PSTH to a 200 ms tone (binned by 10 ms) as the region of interest (ROI). The corresponding raster plot was used to determine the mean onset time of the first spike over $\geq$10 trials.

Maximum firing rates to tones were calculated over a time window equal to the stimulus duration, at the sound level that elicited the highest firing rate. Threshold, dynamic range, and monotonicity were determined from the RLF. Threshold was defined as the decibel (dB) SPL level below which there was at least a 20% increase in firing rate, stepping up from one dB SPL level to the next. Dynamic range was defined as the range between the dB SPL levels where each cell responded at 10 and 90% of its maximum firing rate, calculated by interpolation. Age differences for each of these were assessed with *t* tests. Nonmonotonic neurons were defined as those whose firing rates at the highest dB SPL tested dropped below 50% of their maximum firing rate. Age differences for monotonicity were assessed using the χ^2 test.

Responses to sAM tones were analyzed using three measures: phase-locking to the modulation period (vector strength), firing rate, and power at the modulation frequency (referred to hereafter simply as power). The ROI excluded the first modulation period to ensure that the response to the modulation was examined without contamination by the onset response (Liang et al., 2002). First, vector strength (Goldberg and Brown, 1969) was calculated by treating every spike as a unit vector in a polar coordinate system, where the angle was the instantaneous phase and the mean phase of the response was the direction of the sum of those vectors, normalized to the firing rate. Vector strength (the length of that

mean vector) depends on how tightly the spikes cluster about that one point in the stimulus cycle, varying between zero (e.g., a flat period histogram) and one (all spikes at one phase), and is thus a measure of tight phase-locking. Vector strength was used to construct a temporal MTF (tMTF) (supplemental Fig. 2*A*,*B*, bottom left, available at www.jneurosci.org as supplemental material) and temporal MDF (supplemental Fig. 1*A*,*B*, bottom left, available at www.jneurosci.org as supplemental material). A modified Rayleigh statistic, $z = 2n \times VS^2$, where n is the number of spikes in the ROI and VS is vector strength, was used to determine the level of significant phase-locking (Liang et al., 2002). Vector strength values corresponding to a modified Rayleigh measure of 13.8 were considered statistically significant at a $p < 0.001$ confidence level.

Next, the average firing rate over the entire ROI was determined for each modulation frequency and used to construct a rate MTF (rMTF) (supplemental Fig. 2*A*,*B*, bottom middle, available at www.jneurosci.org as supplemental material) and rate MDF (supplemental Fig. 1*A*,*B*, bottom middle, available at www.jneurosci.org as supplemental material). Firing rate responses to each MD or modulation frequency (MF) were considered significant if they elicited a rate different from that elicited by the lowest tested depth (5% MD) or an unmodulated tone (0% MD), respectively, using a paired t test ($p < 0.05$). Neural rate-based depth detection threshold was defined as the lowest significant MD.

The third measure, power, accounts for both temporal and rate information but does not depend on phase-locked responses and is thus an indicator of how well the spike pattern matches the shape of the sAM envelope. Power was measured by a discrete Fourier transform of spike times using a multitaper process (CHRONUX Toolbox; Cold Spring Harbor). This analysis provides the magnitude of the spiking response at the modulation frequency of the sAM stimulus (Kleinfeld et al., 2002), measured as power (spikes per square seconds per hertz). This measure was used to construct a power MTF (supplemental Fig. 2*A*,*B*, bottom right, available at www.jneurosci.org as supplemental material) and power MDF (supplemental Fig. 1*A*,*B*, bottom right, available at www.jneurosci.org as supplemental material). Power responses to each MD were considered significant if the mean at that depth exceeded the confidence interval of the lowest depth tested. To determine significant frequency, the comparison for each MF was an unmodulated tone binned to match that MF. Neural power-based depth detection threshold was defined as the lowest significant MD. For each measure, age-differences for MTFs or MDFs were assessed with ANCOVAs.

Thresholds were defined as the lowest significant MD (see above for significance) and were computed separately for vector strength, firing rate, and power. The criteria for two of the neurometrics included only "sAM-monotonic" neurons, using criteria similar to those from previous studies (Nelson and Carney, 2007). Neurons were classified as sAM-monotonic either when the MDF contained two consecutive significant MDs and the response to a fully modulated sAM (100% MD) was also significant or when only the 100% MD value achieved significance; this was required to be true based on all three measures (vector strength, firing rate, and power).

For each neuron, tMTFs, rMTFs, and power MTFs were classified based on their sAM MF filter characteristics into one of five categories: low-pass, bandpass, all-pass, high-pass, and band-reject. These were based on a 70% change criterion (across the range of MFs tested, 0.5–100 Hz) in the response above or below the cell's BMF (resulting in an excitatory peak in the MTF) or worst modulation frequency (eliciting the strongest response suppression surrounded by excitatory regions) (Nelson and Carney, 2007).

Neurometrics. Four neurometrics were applied to predict behavioral detection. First, to convert individual neural depth detection into a measure comparable with behavioral detection, d prime (d′) curves for each cell were calculated separately for vector strength, firing rate, and power. Mean z-scores across trials were calculated for each cell at each depth level. For every depth level, d′ was then calculated as $d' = z(MD_{hi}) - z(MD_{low})$, where MD_{low} is the lowest depth tested (5%). Therefore, this is a within-cell neurometric, in that the detection ability of each neuron was compared with its own baseline. Threshold for detection of the signal was defined as d′ = 1. This is equivalent to 67% correct performance when chance is 50%, a criterion that is often used in psychophysical studies.

Second, a population neurometric was constructed from detection thresholds (described above) to reveal the proportion of neurons with responses above threshold across MD. This is a within-cell neurometric, in that the detection ability of each neuron was compared with its own baseline. Curves were created based either on all neurons or on only sAM-monotonic neurons (see above). Thresholds based separately on vector strength, firing rate, and power were used to create separate cumulative histograms. For those cells where no depth produced a response above threshold, threshold was considered to be 110%, and the resulting curves thus did not reach 100% (the limit of a cumulative distribution). This is relevant only for the curves including all neurons, since sAM-monotonic neurons, by definition, have defined thresholds. As this neurometric is constrained by the limits of a cumulative distribution (0–100%), it is likely to deviate in detail from psychometric curves.

Third, a spike-distance metric (Victor and Purpura, 1997) was applied to determine how well spike trains elicited by each depth could be distinguished from baseline [i.e., spike trains elicited by the lowest depth tested (5% MD)]. Like the first two, this is a within-cell neurometric, in that the detection ability of each neuron was compared with its own baseline. This metric reveals the time scale at which detection of sAM is maximal, as it compares spike trains at time scales ranging from 1 to 1000 ms. Dis-similarity between two spike trains is measured as the minimum cost of transforming one spike train into another through several simple operations. The addition of a single spike and the deletion of a single spike each have a cost of 1. In addition, a spike can be shifted in time by an amount dt for a cost of qdt. The parameter q has units of time $^{-1}$, and the quantity $1/q$ is a measure of the temporal resolution of the metric. To measure neural detection for each neuron, distances were calculated between spike trains to determine whether each was closer to baseline or to other spike trains elicited by the same depth. The percentage of correctly classified spike trains was used as the measure of detection, where chance equals 50%.

Fourth, a pooling neurometric was applied that assumes a neural architecture of a single downstream neuron that receives input from all cells (Britten et al., 1992; Shadlen et al., 1996). To measure detection, activity elicited by a baseline stimulus was compared with that elicited by each depth, and a winner-takes-all strategy chose the event with maximum likelihood. Unlike the first three, this is an across-cell neurometric, as each neuron did not serve as its own baseline. The neurometric was applied separately for the three measures (vector strength, firing rate, and power). For each age group, cells were chosen with replacement from the entire pool of sampled neurons, up to the desired pool size (where the maximal pool size was the number of recorded cells). Rather than sampling the same observed responses repeatedly on each trial, we used the Fano factor ρ as a measure of neuronal variability to simulate responses drawn from distributions whose mean and variance matched those of the empirical measurements. Thus, for each MD and for baseline (5% MD), the response for each cell was jittered using $X = \bar{x} + (\sqrt{\bar{x}}\rho \star r)$, where $\bar{x}$ is the mean response magnitude, ρ is the Fano factor, and r is a small random number. Jittered responses were summed, the summed response magnitudes for baseline versus each MD were compared, and a larger value for the higher MD was considered correct detection. This was repeated 20 times (drawing a random subset for each trial), with each comparison equivalent to a single trial, and performance was measured as average correct detection across trials. The neurometric was run 100 times and depicted as mean ± SD, as its performance was quite variable when using only 20 trials (a value chosen to reflect the collected neural data). Our implementation of this model assumes independence across cells, as we were limited by recording from single neurons. As neuronal intercorrelation can diminish the beneficial effect of pooling on performance (Britten et al., 1992), our assumption of independence could predict lower thresholds than if correlations were taken into account. However, this effect is minimal with smaller pool sizes on the scale of those used in this study, and for the low (~0.07) amount of correlation described in ACx (Zohary et al., 1994; Averbeck and Lee, 2004; Eggermont, 2006).

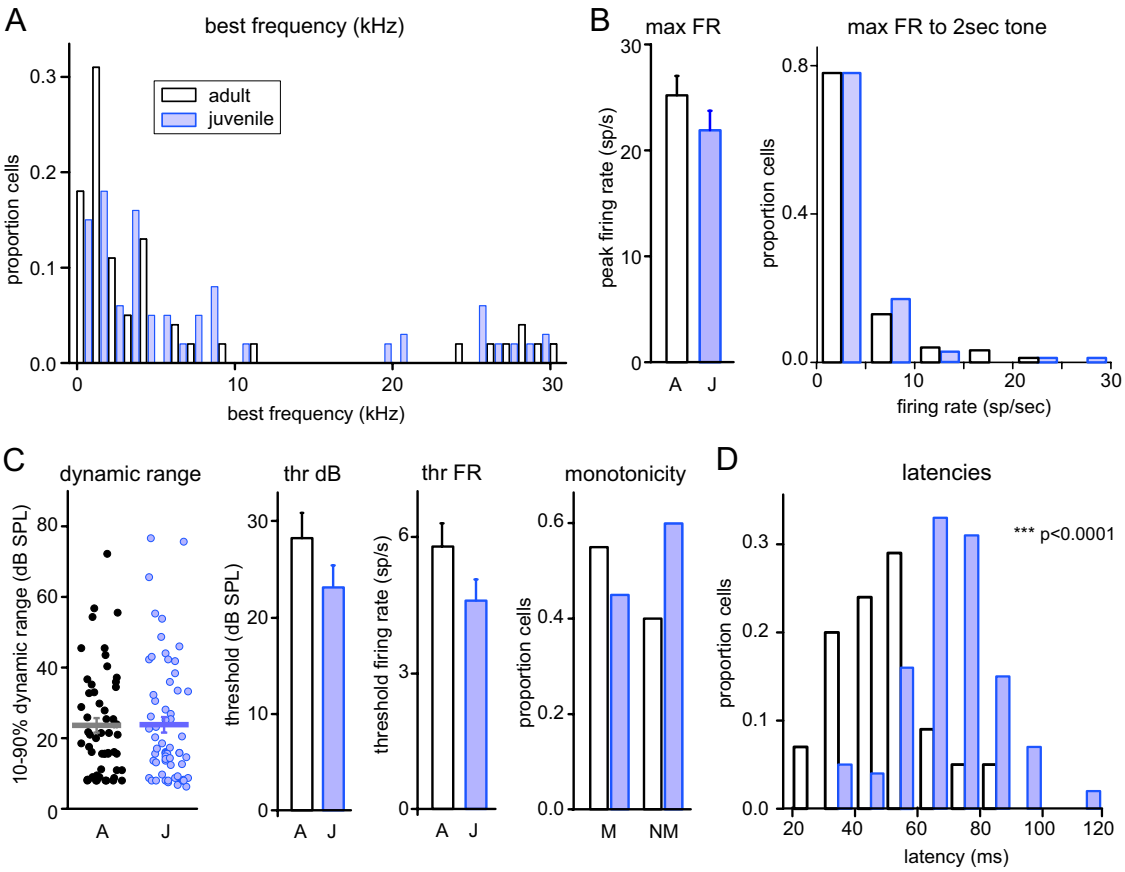

Figure 1. ACx responses to unmodulated tones were mature in juveniles by all measures except first-spike latency. All comparisons were between adult and juvenile groups and measured in response to 200 ms tone pips, unless noted otherwise. ***A***, The distribution of the neuron's BF. ***B***, The maximal firing rate (max FR) elicited by 200 ms (left) or 2 s (right) tone pips at BF. ***C***, Several measures indicating the response to 200 ms tone pips at BF at various sound levels. There were no age differences in the 10–90% dynamic range across sound level, the threshold sound level (thr dB), the firing rate at threshold (thr FR), or the proportion of monotonic (M) to nonmonotonic (NM) cells. ***D***, First-spike latency in response to 200 ms tones at BF was significantly slower in juveniles than in adults. All error bars indicate SEM. A, Adult; J, juvenile.

Results

Responses to unmodulated tones

To establish a developmental baseline for responses to sAM stimuli in juvenile and adult animals, we assessed ACx responses to pure tones. We recorded single units in ACx from 13 adult (P60–P73) and 12 juvenile (P29–P40) awake gerbils. The BF was determined manually, and RLFs were collected using 200 ms tone pips at BF for 55 adult and 62 juvenile neurons. The distribution of BFs was the same for both age groups ($t_{(115)} = 1.15$; $p = 0.25$) (Fig. 1*A*), indicating that we sampled from a similar distribution of cells across the ACx tonotopic axis. By several measures, response properties to 200 ms tone pips were mature by P30. Importantly, the maximum firing rate was equivalent across age groups, both to a 200 ms tone pip and to a 2 s tone pip (200 ms tone: $t_{(115)} = 1.30$, $p = 0.20$; 2 s tone: $t = 0.60$, $p = 0.55$) (Fig. 1*B*), indicating that P30 and adult neurons were equally excitable in response to a static stimulus. This was not the case for firing rate responses to modulated stimuli (see below). As shown in Figure 1*C*, there were no age differences in the neurons' dynamic range ($t_{(115)} = 0.88$; $p = 0.38$), threshold ($t_{(115)} = 1.40$; $p = 0.17$), or firing rate at threshold ($t_{(115)} = 1.57$; $p = 0.12$) or in the ratio of monotonic to nonmonotonic functions ($\chi^2 = 2.37$; $p = 0.12$). However, juvenile neurons had longer latencies to first spike than did adult neurons (adult, 50.4 ± 2.0 ms; juvenile, 69.2 ± 1.9 ms; $t_{(115)} = 6.75$; $p < 0.0001$) (Fig. 1*D*), suggesting that responses to dynamic time-varying stimuli such as sAM would differ across this age range.

Responses to sAM tones: MDFs

The first goal of the study was to evaluate whether sAM depth encoding mechanisms change during the course of development. Since sAM depth detection in gerbils improves late in development (Sarro and Sanes, 2010), we asked whether there was an age-dependent improvement in MD sensitivity in ACx neurons. Responses to sAM tones at varying MDs were obtained at each neuron's BF and BMF. Responses were quantified based on firing rate, vector strength, and power at the sAM modulation frequency. The firing rate ignores temporal properties, whereas vector strength measures phase-locking to the MF (e.g., high values signify discharge at a particular phase of the modulation cycle). Vector strength is normalized by the amount of firing, to avoid spuriously high values for cells with very low firing rates (e.g., when one or two spikes occur at one phase of the response). Power provides the magnitude of the spiking response at the MF independent of phase. Thus, power incorporates both firing rate (response magnitude) and firing pattern information and is well suited to quantify the neural responses that reflect the shape of the sAM envelope.

An example cell is shown in supplemental Figure 1*A* (available at www.jneurosci.org as supplemental material): the MDF depicted was taken at the BMF, which was 2 Hz. The left column depicts raster plots of responses to ten 2 s sAM tones (followed by 1 s silence) across MDs increasing from 5% to 100% sAM depth; the right column shows corresponding modulation period histograms (MPHs). In this cell, a visible response to the sAM enve-

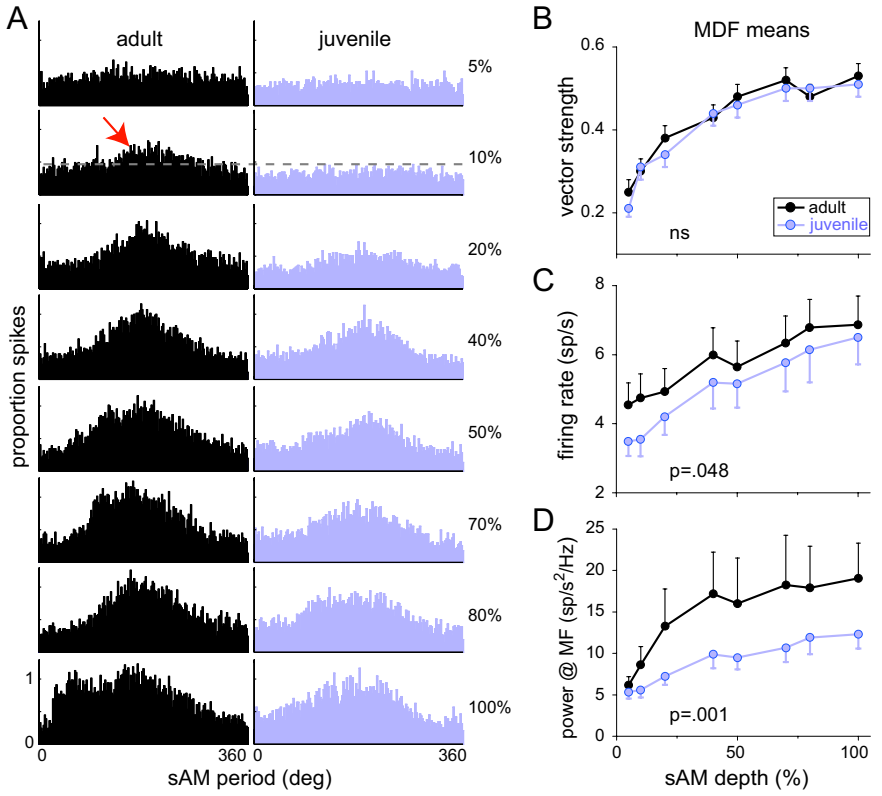

Figure 2. Summary of MDFs for adult and juvenile neurons. ***A***, Population MPHs across the range of tested MDs show a periodicity response emerging clearly at 10% MD in adults (red arrow), but not until 20% or higher in juveniles. ***B–D***, MDF means based on the summary measures firing rate and power were immature in juveniles but were mature based on vector strength, paralleling the age differences seen in MTFs. ns, Not significant.

lope first emerged at 20% MD and became more prominent with sAM depth. This is reflected in the summary measures (supplemental Fig. 1*A*, bottom, available at www.jneurosci.org as supplemental material): vector strength first showed a significant phase-locking at 20% MD; firing rate first increased at 20% MD but was not significantly greater than baseline (5% MD) until 40% MD; power at MF was significantly greater than baseline (5% MD) at 20% MD. The MDF of a non-sAM monotonic responder is depicted in supplemental Figure 1*B* (available at www.jneurosci.org as supplemental material; taken at the BMF, 2 Hz). There was significant phase-locking only at 40 and 50% MD, indicating a nonmonotonic depth response based on vector strength. Neither firing rate nor power differed from baseline (5% MD) at any depth. Responses of the same two neurons to variations in sAM modulation frequency are shown in supplemental Figure 2 (available at www.jneurosci.org as supplemental material); population responses to sAM frequency across age, including categorization based on frequency filter characteristics, are in supplemental Figure 3 (available at www.jneurosci.org as supplemental material).

We quantified and compared population responses to sAM depth for juvenile and adult neurons. MPHs were generated for each depth, then summed across cells and normalized to create pooled MPHs for both groups (Fig. 2*A*) ($n = 69$ adult cells, $n = 67$ juvenile cells). Qualitatively, the temporal pattern of discharge followed the period envelope of the sAM for both groups, and the magnitude of the response increased along with sAM depth. However, a visible envelope response emerged at a shallower MD in adult cells than in juvenile cells (Fig. 2*A*, arrow). At 100% MD, the temporal pattern showed an early peak in the adult population only. This is attributable to several (approximately four) neurons that had short response latencies to the sAM envelope; such neurons were not seen in the juvenile population (data not shown). The qualitative impression that adult cells were more sensitive to sAM depth was quantified for the entire population of recorded neurons. Figure 2*B–D* displays the mean values for each of the three measures. Consistent with age differences seen in the MTFs (supplemental Fig. 2*B*, available at www.jneurosci.org as supplemental material), phase-locking responses (vector strength) were mature, whereas firing rate and power responses were lower than adult levels (vector strength: $F_{(1,1)} = 0.93$, $p = 0.33$; firing rate: $F_{(1,1)} = 3.90$, $p = 0.048$; power: $F_{(1,1)} = 10.21$, $p = 0.001$) (Fig. 2*B*). Thus, for measures that include response magnitude, the population of adult cells was more sensitive to MD.

Neurometric analyses indicate age differences in encoding sAM depth

A major goal of the study was to compare neural sensitivity with behavioral sensitivity. Therefore, we transformed the sAM-evoked spike trains into a form that could be compared directly to the behavioral metric applied to developing gerbils (Sarro and Sanes, 2010). In the following sections, we apply four neurometrics, each with different assumptions about neural processing. The first neurometric examines the detection ability of individual neurons, using the same metric that is typically used to describe behavioral detection (d′). The second neurometric uses only those cells with good detection ability (i.e., sAM-monotonic cells). The third neurometric relies on the detection sensitivity within individual cells but identifies the temporal integration period that most effectively detects sAM. The fourth neurometric pools across all cells and is therefore sensitive to the ability of the population to detect sAM depth but is insensitive to the variation within single cells. For these analyses, only those cells in which responses were obtained to 5–100% MD are presented ($n = 63$ adult cells, $n = 67$ juvenile cells).

Within-cell d′ neurometric

The lower envelope principle states that the limits of psychophysical performance are determined by the most sensitive neurons. That is, an animal's behavioral detection threshold should be reflected in its best neural sensitivity, and only a subset of neurons must have detection thresholds as low as behavioral thresholds (Parker and Newsome, 1998). To compare best neurons across age groups, we therefore examined the detection properties of each neuron. Individual neuron performance was translated into a metric that is comparable with perceptual detection measures, d′, which quantifies the detectability of a signal in the presence of uncertainty and is used routinely in behavioral detection and discrimination tasks. We computed d′ curves for each neuron's sAM depth function, for each of the three measures (vector strength, firing rate, and power; see Materials and Methods). To

do so, the response for each MD was compared with the control response [i.e., to the smallest MD presented (5% MD)]. Here we define d′ = 1 as threshold for detection of the signal. This is equivalent to 67% correct performance when chance is 50%, a criterion that is often used in psychophysical studies.

Individual d′ curves computed from power values are depicted in Figure 3*A*. To focus on threshold performance, each curve is truncated by displaying only that portion that crossed threshold (Fig. 3*A*, horizontal dashed line) until the peak d′ value was attained; all curves are truncated at d′ = 4. Neurons that never reached threshold for any MD are shown in gray. Figure 3*A* suggests that there are a similar number of neurons with sensitive thresholds (<30% depth; vertical dashed line) for adult and juvenile animals (thick lines; 53% adult vs 43% juvenile cells), and the most sensitive neural thresholds were equivalent in juveniles and adults. Figure 3*B* verifies that the distribution of power thresholds does not differ across age groups, and the same was true for vector strength and firing rate (vector strength: $t_{(103)} = 0.1$, $p = 0.94$; firing rate: $t_{(103)} = 1.0$, $p = 0.34$; power: $t_{(107)} = 0.3$, $p = 0.73$). For comparison to the neural thresholds, the behavioral sAM detection thresholds (at d′ = 1) from Sarro and Sanes (2010) are replotted above the bars in Figure 3*B*. Although adult behavioral thresholds are lower than juveniles by ~15% MD, neither age group performs as well as its best neurons. Therefore, based on responses in ACx, the lower envelope principle does not explain the observed behavioral difference across age.

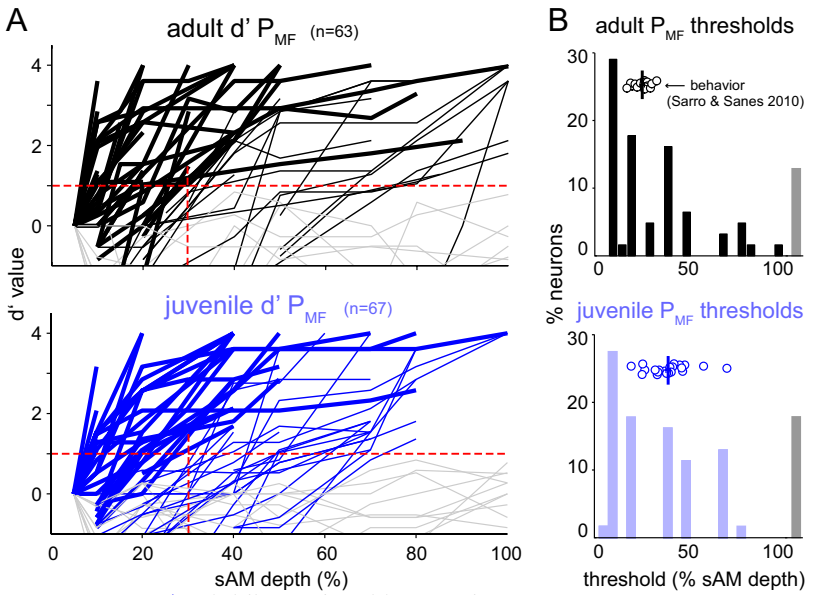

Figure 3. Neural d′-based MD thresholds do not differ across age. ***A***, Individual neural d′ curves calculated from power at the modulation frequency (P_{MF}) are truncated by displaying only that portion that crossed threshold (horizontal dashed line) until the peak d′ value was attained. All curves are truncated at d′ = 4.0. Neurons whose curves never reached threshold are in gray. Across age, there were equivalent numbers of cells with sensitive thresholds: cells with thresholds <30%MD (vertical dashed line) are shown with thick lines. ***B***, The distribution of power-based d′ thresholds do not differ across age ($p = 0.94$), and there are cells with equally low thresholds in both age groups, indicating that the lower envelope principle at the level of ACx cannot account for perceptual age differences in MD threshold. Gray bars indicate cells that never reached threshold. Behavioral sAM depth detection thresholds [extrapolated and replotted from Sarro and Sanes (2010), their Fig. 5*A*] are overlaid as open circles with mean performance indicated by the dark vertical lines. Although adults have lower behavioral thresholds by ~15% MD, neither group achieves detection thresholds as low as the best neurons.

There are certain caveats associated with this comparison of neural and behavioral data. The behavioral thresholds to sAM depth were obtained using a broadband noise carrier, whereas the neural thresholds were obtained using a tone carrier at each cell's BF. Had we characterized neurons with a noise carrier, the literature suggests that the population of neurons would have displayed greater sensitivity to sAM (Eggermont, 1994). Had the behavioral thresholds been obtained with a tone carrier, animals would probably have displayed poorer sensitivity to sAM depth (Strickland and Viemeister, 1997). Therefore, this comparison is likely to underestimate the difference between neural and behavioral thresholds. A second caution is that the neural thresholds were obtained in untrained, passively listening animals, whereas the behavioral thresholds represent mean performance for each animal after several days of experience (Sarro and Sanes, 2010). As the stimulus selectivity of ACx neurons are known to be influenced during performance of a previously trained task (Fritz et al., 2003), the responses of cells in untrained animals may not reflect trained behavior appropriately across development.

Within-cell threshold-based neurometric

We next assessed the population activity at each age under the constraints of three assumptions. The first assumption is an extension of the lower envelope principle: if the limits of behavioral detection are set by the thresholds of the most sensitive cells, then the shape of a psychometric function for sAM depth detection should arise from the population of neuronal thresholds (Delgutte, 1995). The second assumption is that each cell is equally weighted, as the analysis is a cumulative distribution of single-cell thresholds across each sAM depth. The third assumption explores the possibility that in order for a neuron to contribute to sAM depth detection, it must respond monotonically to depth. Monotonic functions to increasing depth are observed frequently in the auditory brainstem (Joris et al., 2004) and have served as a criterion in a previous comparison of neuronal and psychophysical detection (Nelson and Carney, 2007). The reason for excluding nonmonotonic neurons is that they do not provide a reliable discharge characteristic as the parameter of interest is varied. This creates a within-cell analysis, as each neuron's response is compared with its own baseline response to yield a depth detection threshold. In ACx, the responses to sAM are quite variable across neurons, so this approach was chosen to assess whether sAM monotonicity within neurons was essential for MD detection. We tested this assumption explicitly by selecting only those cells with approximately monotonic sAM functions and comparing the result to that generated by the inclusion of all cells.

We computed MD detection thresholds for each neuron (see Materials and Methods) and created cumulative histograms to display population performance. The neurometric was constructed by including either all cells or only those cells that were approximately monotonic to sAM depth (sAM-monotonic; see Materials and Methods). Thresholds based on power are shown for two example cells from juvenile animals in Figure 4*A*; these cells are representative of sAM-nonmonotonic and sAM-monotonic neurons for both age groups. On the left is a cell that responded vigorously to a static tone pip at BF (Fig. 4*A*, top) but

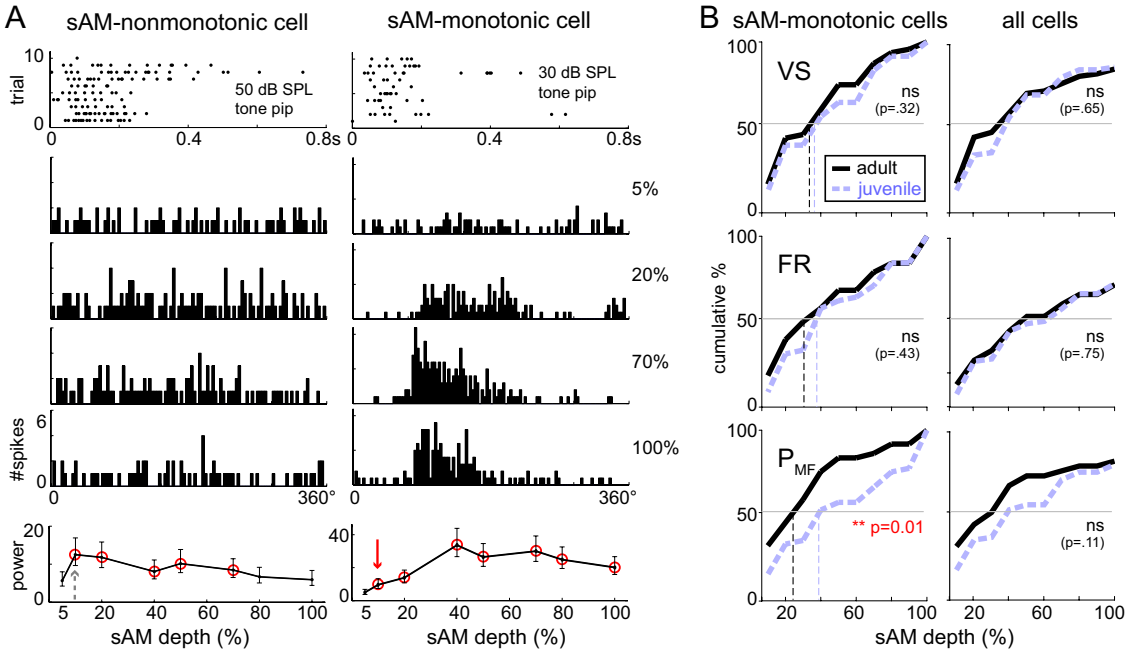

Figure 4. A within-cell neurometric based on the cumulative distribution of MD thresholds only reveals superior adult performance when sAM-nonmonotonic neurons are excluded. ***A***, This illustrates how thresholds are chosen for inclusion in the cumulative distribution of this neurometric. Shown here are examples of sAM-nonmonotonic (left) and sAM-monotonic (right) neurons, which were nonmonotonic or monotonic, respectively, based on MD. The top row contains raster plots of responses to 10 presentations of a 2 s tone pip at BF, indicating strong responses in both cells. The middle four rows show MPHs across MD (collected at BF and BMF). The nonmonotonic neuron did not display MD-evoked responses, whereas the monotonic neuron responded more strongly as MD increased. The bottom row depicts power across MD, with significant responses circled in red. The cell on the right, but not the cell on the left, was considered monotonic (see criteria in Materials and Methods). Thresholds are indicated by gray and red arrows, for the nonmonotonic and monotonic cell, respectively. ***B***, Cumulative distributions of MD detection thresholds from either monotonic cells (left) or all cells (right). For power at the modulation frequency (P_{MF}), but not for vector strength (VS) or firing rate (FR), the monotonic curve for juvenile neurons was shifted significantly to the right compared with adult neurons. This was consistent with age differences in behavioral performance. Cumulative histograms incorporating all neurons showed no age differences for any of the three measures. ns, Not significant.

responded poorly to a sAM tone at BF and was nonmonotonic as depth increased. This cell did not show significantly greater power at 100% MD than baseline, so it was not included in the sAM-monotonic power neurometric. On the right is a cell that responded both to a tone pip and a sAM tone, and was monotonic with respect to MD. Its threshold was 10% MD based on power (Fig. 4*A*, arrow). Across the populations, there were similar proportions of cells with these properties for both age groups: 37% of adult and 43% of juvenile neurons were sAM-monotonic.

Figure 4*B* (left) shows cumulative histograms of thresholds from sAM-monotonic cells, constructed separately for each of the metrics. Adult curves are above juvenile for all metrics, but only significantly so for the power metric. This analysis predicts that juvenile animals should perform nearly as well as adults if either vector strength or firing rate information is being used (e.g., an ~5% rightward shift in juvenile cumulative distribution), which is not consistent with the behavioral data (Sarro and Sanes, 2010). However, if animals make use of both temporal and rate information, as represented by power, our results predict that behavioral thresholds will be significantly worse for juvenile animals (e.g., an ~15% rightward shift in juvenile cumulative distribution). When cumulative histograms were constructed using thresholds from all cells, there were no significant age differences (Fig. 4*B*, right). The age difference from this approach thus relies on the exclusion of cells that are nonmonotonic for sAM depth.

Within-cell integration-time neurometric

A second neurometric was used to identify the temporal integration period that best detected sAM depth. A spike-distance metric (Victor and Purpura, 1997) quantified, for each neuron, the dissimilarity between spike trains evoked by sAM versus spike trains evoked by the smallest MD tested. Therefore, like the first neurometric (Fig. 4), this approach is sensitive to within-cell monotonicity or other variations across MD and weights each neuron equally. For this reason, we constructed two versions of the neurometric, using either all cells or a subset of sAM-monotonic cells (see Materials and Methods).

To calculate correct detection, the distance between spike trains elicited by sAM versus background was compared with the distance between the spike trains elicited by either stimulus alone. A larger distance between stimuli than within stimuli indicated correct detection. For each cell, we computed correct detection for each MD compared with the lowest depth tested (5% MD). Averages are plotted as a function of increasingly longer analysis windows within the entire spike train, ranging from 1 to 1000 ms (Fig. 5*A*). As expected, detection was better for higher MDs (e.g., Fig. 5*A* depicts 100% and 20% MD). Performance was best at longer time scales (above about 100 ms), indicating that fine temporal structure contributed little to spike train dissimilarity. When all cells were included, there was no age difference in detection based on this metric at any time scale. However, when only sAM-monotonic cells were included, a clear age difference emerged for longer time scales (Fig. 5*A*, right). The longest time scale (1000 ms) reflects contributions of firing rate and is thus comparable to the firing rate measure. Time scales near the periodicity of the sAM signal (200–500 ms) are comparable to power. Consistent with other analyses, the greatest age differences were seen at these longer time scales. However the time scale that maximized detection was mature in juveniles, as maximal detection

occurred at longer time scales in both age groups. Thus, similar integration times underlie detection in juveniles and adults. Figure 5*B* translates this analysis into a neurometric representation by plotting detection performance at just one time scale (1000 ms) as a function of sAM depth. Overall performance was better when nonmonotonic cells were excluded, and an age difference indicates that, behaviorally, adult thresholds should be >10% MD lower than those of juveniles.

One assumption of this approach is that each cell is equally weighted. The analysis is an average of depth detection curves, where the response at each depth is compared with each neuron's own baseline response (within-cell comparison) to yield detection performance. However, if each of these cells were to converge on a single target, the output would be dominated by those input neurons that displayed the strongest response to depth, rather than equally weighted as in this average. That is, each neuron's response would no longer be referenced to its own baseline response. Rather, the sum of all baseline responses would be the reference for the sum of all responses at any given depth. We therefore applied a neurometric that pools across all cells in this manner.

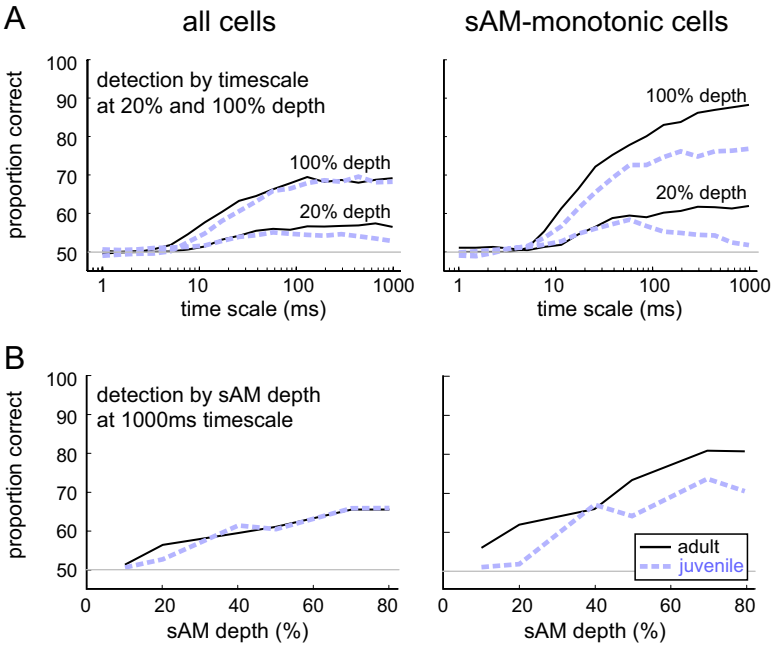

Figure 5. A within-cell integration-time neurometric only displayed adult performance superior to that of juveniles at long time scales and when nonmonotonic neurons were excluded. ***A***, Mean neural detection performance is shown across time scales ranging from 1 ms (where precise timing differentiates spike trains) to 1000 ms (where rate differentiates spike trains). Detection was better at longer time scales, and better for larger MDs (100%) than smaller MDs (20%). An age difference emerged at longer time scales, but only when nonmonotonic cells were excluded (right). ***B***, At a long time scale (1000 ms), detection across MD was better in adults versus juveniles only when nonmonotonic cells were excluded (right).

Across-cell pooling neurometric

The final neurometric is a pooling model that is based on a neural architecture in which the readout of the system is a downstream neuron receiving the inputs from all cells in the measured sample. This convergence is computed by summing the responses of all cells for any given MD. Thus, cells with larger response magnitudes will dominate the summed responses. Unlike the previous neurometric, this approach is not sensitive to within-cell monotonicity or other variations across MD. Rather it measures the ability of the population to detect sAM depth based on convergence (Britten et al., 1992; Shadlen et al., 1996).

For each MD, the jittered (see Materials and Methods) response magnitude (based on firing rate, vector strength, or power) across all cells was summed and compared to the summed response magnitude at 5% MD, where a higher sum was considered a correct detection. This was repeated 20 times (drawing a random subset for each trial), with each comparison equivalent to a single trial, and performance was measured as average correct detection across trials. The neurometric was run 100 times and depicted as mean ± SD, as its performance was quite variable when using only 20 trials. Figure 6*A* (bottom, pale lines in power plot) illustrates how summed values from each depth are compared with the lowest depth; each depth must be only just larger than baseline (red dashed line) to yield a correct detection. The summed functions approximate the mean power functions shown in Figure 2*D*. A gradual increase in power (Fig. 6*A*, pale lines) is converted by pooling into a sharp rise in detection performance (Fig. 6*A*, dark lines). This also has the effect of reducing the magnitude of an age difference once the response at any depth is sufficiently above baseline (i.e., for higher MDs), as the neurometric asymptotes.

Figure 6*A* shows the performance of this neurometric for all juvenile and adult cells, separately for each of the three measures. For all measures, performance reached an asymptote at 40% MD, as the summed responses were already reliably above baseline. Below 40% MD, juvenile cells did not detect sAM from background as well as adult cells, most clearly illustrated for firing rate and power. With this neurometric, it is possible to ask how many cells are necessary to yield maximal performance by including only a subset of cells from each age group (Britten et al., 1992; Shadlen et al., 1996). Figure 6*B* shows the effect of pool size on detection performance at 10, 20, and 30% MD. Above 10% MD, reducing the number of cells included in the neurometric decreased the mean performance and increased the variability for both age groups. At 10% MD, an age difference emerged: adult performance improved with increasing pool size, but juvenile did not, for firing rate and power. This pooling neurometric predicts that adult gerbils would exhibit near-perfect detection at 10% depth, whereas juveniles would perform significantly above chance (Fig. 6*B*, solid horizontal lines) only at larger depths. Changing pool size indicates that a pool of ~30 neurons is sufficient for maximal detection. It also suggests that increasing the pool size only improves detection for values that are above threshold.

Discussion

This study addressed whether immature sAM detection measured behaviorally (Sarro and Sanes, 2010) can be explained by immature ACx encoding. Our results demonstrated a significant developmental delay of sAM-evoked responses in ACx. Specifically, firing rate and power at the modulation frequency were greater in adult neurons, as a function of sAM depth or frequency (Fig. 2 and supplemental Fig. 3, available at www.jneurosci.org as supplemental material); in contrast, phase-locking (vector

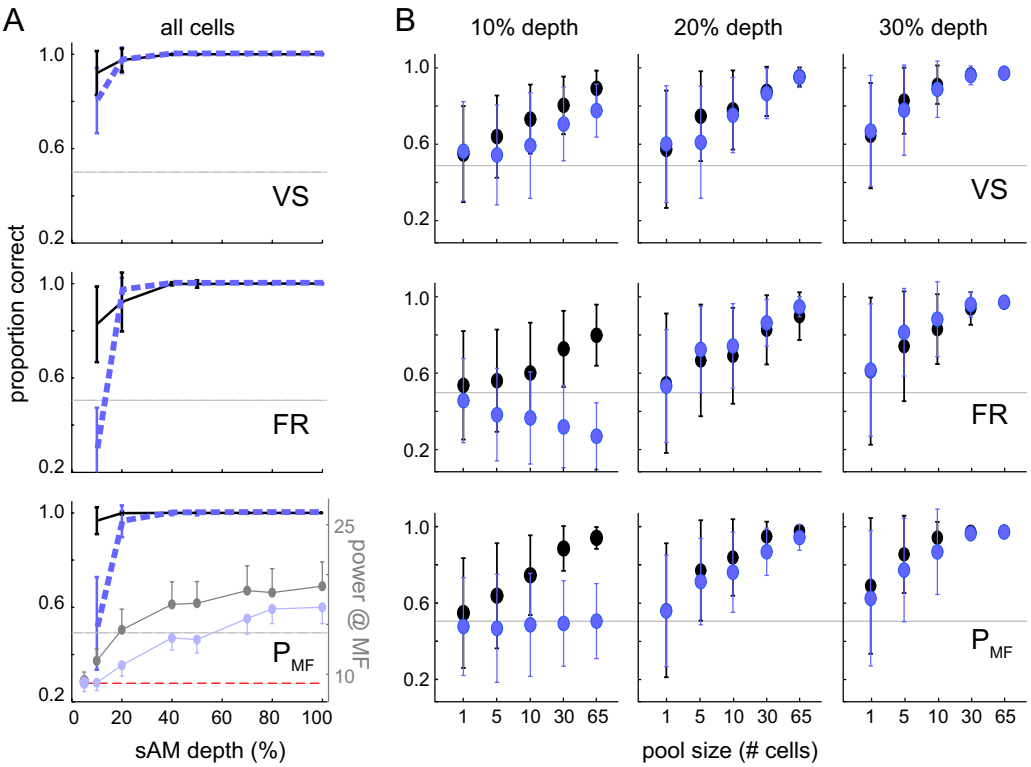

Figure 6. An across-neuron pooling neurometric that sums across cells does not rely on within-cell monotonicity and thus included both nonmonotonic and monotonic cells. This neurometric displayed age differences for all measures except vector strength. ***A***, Detection performance based on the three measures is plotted across MD, showing better adult than juvenile sAM detection at MDs $<$20%. The pale lines in the bottom plot show overlaid summed power (P_{MF}) values that were used to calculate detection performance, where each depth must be only just larger than baseline (red dashed line) to yield correct detection. Note that a gradual increase in summed P_{MF} (pale lines) is converted by pooling into a sharp rise in detection performance (dark lines). ***B***, For 20% and 30% MD, increasing pool size up to ~30 cells increased performance and reduced variability for both adults and juveniles. For 10% MD, increasing pool size did not improve juvenile detection for firing rate and power.

strength) was adult like in juveniles. Therefore, maturational improvements in perceptual performance could be mediated by developmental changes to both response magnitude and periodicity. This is consistent with the finding that sAM processing is better characterized by a metric that mirrors the envelope shape of the sAM rather than one that is locked to a specific phase of the sAM (Bernstein and Trahiotis, 2003; Malone et al., 2007).

Our premise was that those coding properties that covary with perceptual performance across ages are more likely to support the behavior than those that are only correlated in adulthood. Three of four different neurometric analyses displayed an age-dependent improvement in sAM detection thresholds when based on firing rate or power (Figs. 4–6), consistent with behavioral sAM detection in developing gerbils (Sarro and Sanes, 2010). A longer maturational time course for firing rate is also consistent with findings that both spontaneous and stimulus-evoked firing are considerably smaller in young versus adult cats (Huttenlocher, 1967; Eggermont, 1991). Since these conclusions draw from neurometric analyses with different assumptions, we next consider the relative merits of each.

Relevance of each neurometric analysis to perceptual development

Frequently, performance of the best single neurons is as good as or better than behavior (Britten et al., 1992; Hernandez et al., 2000; Wang et al., 2007). Thus, the first neurometric allowed a direct comparison of individual neurons with psychophysical curves, as both are quantified using the signal detection measure, d′. This is a within-cell comparison, rather than a population metric, insofar as detection at each depth is referenced to the baseline response of that neuron. The assumption is that the limits of psychophysical performance are determined by the most sensitive neurons (i.e., the lower envelope principle), and only a subset of neurons must have detection thresholds as low as behavioral thresholds (Barlow, 1995; Parker and Newsome, 1998). Behavioral thresholds are, in fact, between those of the best and worst single neurons, with adult behavioral thresholds closer to those of the best neurons (Fig. 3*B*). We observed no age difference in the thresholds of the best neurons, indicating that the difference between behavioral thresholds of juveniles and adults is not simply a consequence of the information available in the best neurons.

One interpretation of this result is that juvenile and adult animals do not use the sensory representation of sAM at the level of ACx in an equivalent manner. This concept has been demonstrated in behaving primates: somatosensory cortical responses covary with stimulus strength, but not with trial-to-trial perceptual judgments, whereas frontal cortex activity correlates with the outcome of each trial (de Lafuente and Romo, 2005). Thus, sensory cortices are likely to be involved primarily with encoding (Hernandez et al., 2000; Lemus et al., 2009a), whereas higher cortical areas that receive inputs from sensory areas and send outputs to motor areas are involved in perceptual decisions (Kim and Shadlen, 1999; Lee et al., 2009; Lemus et al., 2009b). Thus, it is possible that immature perceptual performance is attributable to immature decoding of sensory information.

The second neurometric again made use of within-cell comparisons in which a significant increase in the value of a coding

property (vector strength, firing rate, power) with respect to baseline was accepted as the cell's threshold. In this case, however, a key assumption was that only neurons that respond monotonically to depth could contribute reliably to sAM detection. Neural detection thresholds of the populations were then accumulated to predict performance across the entire range of MDs (Fig. 4). For the power measure, the cumulative histogram of detection thresholds for juvenile neurons was shifted to the right compared to adult neurons, consistent with age differences in behavioral performance. Since there was no difference for vector strength or firing rate, this result emphasizes the importance of encoding stimulus envelope (Bernstein and Trahiotis, 2003; Malone et al., 2007).

The third neurometric identified the temporal integration period that most effectively detects sAM (Fig. 5) and also relied on within-cell comparisons. This metric displayed good performance at integration times that were in accordance with firing rate and power coding properties and agreed with the other within-cell population neurometric by predicting threshold and asymptotic age differences only with monotonic cells.

One concern with these analyses is the underlying assumption that each neuron contributes equally to sAM detection. If only the most sensitive neurons contribute, a population analysis incorporating less sensitive cells can decrease the signal-to-noise ratio across neurons and wash out the contribution of the best cells (Purushothaman and Bradley, 2005; Wang et al., 2007). This was likely the case for the within-cell neurometrics, where no age difference existed when all cells were included (Figs. 4, 5). Thus, the threshold-based and integration-time analyses identified an age difference only when restricted to cells that were reliable depth detectors.

The above neurometric analyses each require a neural mechanism that can selectively access reliable sAM detectors. However, there is no evidence that such a mechanism exists. Therefore, an alternative approach is to use a pooling neurometric model that assumes a synaptically plausible downstream decoder cell based on anatomical convergence and synaptic summation (Britten et al., 1992; Shadlen et al., 1996; Parker and Newsome, 1998). This model is more robust to noise because summation produces unequal weighting and small responses are dominated by larger ones (in contrast to the equal weighting of the within-cell neurometrics). Additionally, it does not rely on input neurons being individually well tuned, as long as the population activity is tuned. The pooling neurometric produced better sAM detection for adult neurons at 10% MD, compared to juveniles (Fig. 6), consistent with age differences in behavioral performance. However, there was no difference at higher MDs because detection asymptoted even though the responses of individual neurons continued to increase (Fig. 6*A*, bottom, thick dark vs thin pale lines). Nevertheless, when assessing the entire population, a mechanism that pools across all cells matches behavior better than one that assumes that each cell must be an individually effective detector.

For gerbils, sAM detection threshold varies with age and training. When practice is limited to assess developmental differences, adult thresholds are ~30%, whereas juvenile thresholds are ~45% (Sarro and Sanes, 2010). Neurometrics that suggest immature ACx encoding in juveniles (Figs. 4–6) are consistent with the observed ~15% difference in behavioral thresholds. Since the neural detection thresholds obtained here (≤10% for adults) (Fig. 6*A*) are much better than those measured behaviorally with little practice, it is possible that they reflect the ultimate performance that can be achieved through perceptual learning (Wright and Zhang, 2009). In fact, we have observed adult thresholds ≤10% with practice (M. J. Rosen, E. C. Sarro, and Sanes, unpublished observations). This value is consistent with adult sAM detection thresholds in other species [human, 6–10% (Viemeister, 1979; Hall and Grose, 1994); chinchilla, ~9% (Salvi et al., 1982); rat, ~15% (Kelly et al., 2006)].

Potential contribution of subcortical and higher cortical factors

Our intent was to assess sensory information available to higher decision-making regions. Therefore, we measured encoding in ACx because it inherits and filters subcortical inputs, thus reflecting developmental differences established lower in the sensory hierarchy. Moreover, ACx provides input to areas that decode sensory information: multisensory, premotor, and decision-making regions of cortex (Budinger et al., 2000, 2006; Kaas and Hackett, 2000).

It is possible that developmental differences in ACx reflect an immature ascending pathway. For example, sAM responses in inferior colliculus display a prolonged period of development (Heil et al., 1995; Thornton et al., 1999). However, a significant descending projection from ACx to midbrain and thalamus influences encoding and plasticity at those levels (Coomes Peterson and Schofield, 2007; Suga, 2008; Bajo et al., 2010; Nakamoto et al., 2010). Therefore, evaluating the contribution of brainstem coding is, itself, complicated by corticofugal modulation.

It is also possible that immature performance is influenced by cognitive factors. Active participation in an auditory task, and the increased attention that it leverages, can influence encoding (Fritz et al., 2003, 2007). Attention is reported to produce modest increases (Scott et al., 2007) or decreases (Otazu et al., 2009) in sound-evoked ACx responses during task performance. Although attention, context, motivation, and arousal are not addressed by this study, we found no developmental differences in behavioral measures commonly correlated with attention (e.g., false-alarm rate and asymptotic performance) (Sarro and Sanes, 2010). Therefore, it is likely that the maturation of sensory encoding can be measured in awake, passively listening animals.

Comparison of sAM coding to static stimulus coding

Response properties to different stimuli (e.g., static vs modulated envelopes) may mature at different rates because the mechanisms that determine those properties have different maturation rates. Our data show that responses to tones with static envelopes mature earlier than to modulated envelopes. It is known that simple response properties such as BF and bandwidth are likely established by ascending and intracortical excitatory connections (Kaur et al., 2004; Metherate et al., 2005; Liu et al., 2007), whereas responses to more complex stimuli such as frequency modulations are influenced by intracortical inhibition (Zhang et al., 2003; Razak and Fuzessery, 2007a). Although the mechanisms of sAM tuning are not well understood, sAM responses in ACx neurons are related to sound level monotonicity (Malone et al., 2007), which at the level of the inferior colliculus is refined by local inhibition (Sivaramakrishnan et al., 2004). Local cortical inhibitory circuits mature fairly late in development (>P24) (Gao et al., 1999; Chang et al., 2005), suggesting that the slow maturation of sAM may be caused by the gradual development of inhibition in ACx.

References

Averbeck BB, Lee D (2004) Coding and transmission of information by neural ensembles. Trends Neurosci 27:225–230.

Bajo VM, Nodal FR, Moore DR, King AJ (2010) The descending corticocol-

licular pathway mediates learning-induced auditory plasticity. Nat Neurosci 13:253–260.
Banai K, Sabin AT, Kraus N, Wright BA (2007) The development of sensitivity to amplitude and frequency modulation follow distinct time courses. Paper presented at Conference of the Association for Research in Otolaryngology, Denver, CO.
Barlow H (1995) The neuron doctrine in perception. In: The cognitive neurosciences (Gazzaniga MS, ed), pp. 415–434. Cambridge, MA: MIT.
Bernstein LR, Trahiotis C (2003) Processing of interaural temporal disparities with both "transposed" and conventional stimuli. In: Auditory signal processing: physiology, psychoacoustics, and models (Pressnitzer D, De Cheveigne A, McAdams S, Collet L, eds), pp. 377–389. New York: Springer.
Bonham BH, Cheung SW, Godey B, Schreiner CE (2004) Spatial organization of frequency response areas and rate/level functions in the developing AI. J Neurophysiol 91:841–854.
Britten KH, Shadlen MN, Newsome WT, Movshon JA (1992) The analysis of visual motion: a comparison of neuronal and psychophysical performance. J Neurosci 12:4745–4765.
Brown TA, Harrison RV (2010) Postnatal development of neuronal responses to frequency-modulated tones in chinchilla auditory cortex. Brain Res 1309:29–39.
Budinger E, Heil P, Scheich H (2000) Functional organization of auditory cortex in the Mongolian gerbil (*Meriones unguiculatus*). III. Anatomical subdivisions and corticocortical connections. Eur J Neurosci 12:2425–2451.
Budinger E, Heil P, Hess A, Scheich H (2006) Multisensory processing via early cortical stages: connections of the primary auditory cortical field with other sensory systems. Neuroscience 143:1065–1083.
Chang EF, Bao S, Imaizumi K, Schreiner CE, Merzenich MM (2005) Development of spectral and temporal response selectivity in the auditory cortex. Proc Natl Acad Sci U S A 102:16460–16465.
Coomes Peterson D, Schofield BR (2007) Projections from auditory cortex contact ascending pathways that originate in the superior olive and inferior colliculus. Hear Res 232:67–77.
de Lafuente V, Romo R (2005) Neuronal correlates of subjective sensory experience. Nat Neurosci 8:1698–1703.
Delgutte B (1995) Physiological models for basic auditory percepts. In: Auditory computation (Hawkins HL, McMullen TA, Popper A, Fay RR, eds), pp 157–220. New York: Springer.
Eggermont JJ (1991) Maturational aspects of periodicity coding in cat primary auditory cortex. Hear Res 57:45–56.
Eggermont JJ (1994) Temporal modulation transfer functions for AM and FM stimuli in cat auditory cortex. Effects of carrier type, modulating waveform and intensity. Hear Res 74:51–66.
Eggermont JJ (2006) Properties of correlated neural activity clusters in cat auditory cortex resemble those of neural assemblies. J Neurophysiol 96:746–764.
Elliott DN, Trahiotis C (1972) Cortical lesions and auditory discrimination. Psychol Bull 77:198–222.
Fritz J, Shamma S, Elhilali M, Klein D (2003) Rapid task-related plasticity of spectrotemporal receptive fields in primary auditory cortex. Nat Neurosci 6:1216–1223.
Fritz JB, Elhilali M, Shamma SA (2007) Adaptive changes in cortical receptive fields induced by attention to complex sounds. J Neurophysiol 98:2337–2346.
Gaese BH, Ostwald J (2001) Anesthesia changes frequency tuning of neurons in the rat primary auditory cortex. J Neurophysiol 86:1062–1066.
Gao WJ, Newman DE, Wormington AB, Pallas SL (1999) Development of inhibitory circuitry in visual and auditory cortex of postnatal ferrets: immunocytochemical localization of GABAergic neurons. J Comp Neurol 409:261–273.
Goldberg JM, Brown PB (1969) Response of binaural neurons of dog superior olivary complex to dichotic tonal stimuli: some physiological mechanisms of sound localization. J Neurophysiol 32:613–636.
Hall JW 3rd, Grose JH (1994) Development of temporal resolution in children as measured by the temporal modulation transfer function. J Acoust Soc Am 96:150–154.
Heil P, Schulze H, Langner G (1995) Ontogenetic development of periodicity coding in the inferior colliculus of the Mongolian gerbil. Aud Neurosci 1:363–383.
Hernandez A, Zainos A, Romo R (2000) Neuronal correlates of sensory discrimination in the somatosensory cortex. Proc Natl Acad Sci U S A 97:6191–6196.
Huttenlocher PR (1967) Development of cortical neuronal activity in the neonatal cat. Exp Neurol 17:247–262.
Joris PX, Schreiner CE, Rees A (2004) Neural processing of amplitude-modulated sounds. Physiol Rev 84:541–577.
Kaas JH, Hackett TA (2000) Subdivisions of auditory cortex and processing streams in primates. Proc Natl Acad Sci U S A 97:11793–11799.
Kaur S, Lazar R, Metherate R (2004) Intracortical pathways determine breadth of subthreshold frequency receptive fields in primary auditory cortex. J Neurophysiol 91:2551–2567.
Kelly JB, Cooke JE, Gilbride PC, Mitchell C, Zhang H (2006) Behavioral limits of auditory temporal resolution in the rat: amplitude modulation and duration discrimination. J Comp Psychol 120:98–105.
Kim JN, Shadlen MN (1999) Neural correlates of a decision in the dorsolateral prefrontal cortex of the macaque. Nat Neurosci 2:176–185.
Kleinfeld D, Sachdev RN, Merchant LM, Jarvis MR, Ebner FF (2002) Adaptive filtering of vibrissa input in motor cortex of rat. Neuron 34:1021–1034.
Kohlrausch A, Fassel R, Dau T (2000) The influence of carrier level and frequency on modulation and beat-detection thresholds for sinusoidal carriers. J Acoust Soc Am 108:723–734.
Krause JC, Braida LD (2004) Acoustic properties of naturally produced clear speech at normal speaking rates. J Acoust Soc Am 115:362–378.
Lee JH, Russ BE, Orr LE, Cohen YE (2009) Prefrontal activity predicts monkeys' decisions during an auditory category task. Front Integr Neurosci 3:16.
Lemus L, Hernandez A, Romo R (2009a) Neural codes for perceptual discrimination of acoustic flutter in the primate auditory cortex. Proc Natl Acad Sci U S A 106:9471–9476.
Lemus L, Hernandez A, Romo R (2009b) Neural encoding of auditory discrimination in ventral premotor cortex. Proc Natl Acad Sci U S A 106:14640–14645.
Liang L, Lu T, Wang X (2002) Neural representations of sinusoidal amplitude and frequency modulations in the primary auditory cortex of awake primates. J Neurophysiol 87:2237–2261.
Liu BH, Wu GK, Arbuckle R, Tao HW, Zhang LI (2007) Defining cortical frequency tuning with recurrent excitatory circuitry. Nat Neurosci 10:1594–1600.
Malone BJ, Semple MN (2001) Effects of auditory stimulus context on the representation of frequency in the gerbil inferior colliculus. J Neurophysiol 86:1113–1130.
Malone BJ, Scott BH, Semple MN (2007) Dynamic amplitude coding in the auditory cortex of awake rhesus macaques. J Neurophysiol 98:1451–1474.
Malone BJ, Scott BH, Semple MN (2010) Temporal codes for amplitude contrast in auditory cortex. J Neurosci 30:767–784.
Metherate R, Kaur S, Kawai H, Lazar R, Liang K, Rose HJ (2005) Spectral integration in auditory cortex: mechanisms and modulation. Hear Res 206:146–158.
Middlebrooks JC (2008) Auditory cortex phase locking to amplitude-modulated cochlear implant pulse trains. J Neurophysiol 100:76–91.
Nakamoto KT, Shackleton TM, Palmer AR (2010) Responses in the inferior colliculus of the guinea pig to concurrent harmonic series and the effect of inactivation of descending controls. J Neurophysiol 103:2050–2061.
Nelson PC, Carney LH (2007) Neural rate and timing cues for detection and discrimination of amplitude-modulated tones in the awake rabbit inferior colliculus. J Neurophysiol 97:522–539.
Ohl FW, Wetzel W, Wagner T, Rech A, Scheich H (1999) Bilateral ablation of auditory cortex in Mongolian gerbil affects discrimination of frequency modulated tones but not of pure tones. Learn Mem 6:347–362.
Otazu GH, Tai LH, Yang Y, Zador AM (2009) Engaging in an auditory task suppresses responses in auditory cortex. Nat Neurosci 12:646–654.
Parker AJ, Newsome WT (1998) Sense and the single neuron: probing the physiology of perception. Annu Rev Neurosci 21:227–277.
Pienkowski M, Harrison RV (2005) Tone frequency maps and receptive fields in the developing chinchilla auditory cortex. J Neurophysiol 93:454–466.
Pincas J, Jackson PJ (2006) Amplitude modulation of turbulence noise by voicing in fricatives. J Acoust Soc Am 120:3966–3977.
Purushothaman G, Bradley DC (2005) Neural population code for fine perceptual decisions in area MT. Nat Neurosci 8:99–106.
Razak KA, Fuzessery ZM (2007a) Development of inhibitory mechanisms

underlying selectivity for the rate and direction of frequency-modulated sweeps in the auditory cortex. J Neurosci 27:1769–1781.

Razak KA, Fuzessery ZM (2007b) Development of functional organization of the pallid bat auditory cortex. Hear Res 228:69–81.

Rosen S (1992) Temporal information in speech: acoustic, auditory and linguistic aspects. Philos Trans R Soc Lond B Biol Sci 336:367–373.

Salvi RJ, Giraudi DM, Henderson D, Hamernik RP (1982) Detection of sinusoidally amplitude modulated noise by the chinchilla. J Acoust Soc Am 71:424–429.

Sarro EC, Sanes DH (2010) Prolonged maturation of auditory perception and learning in gerbils. Dev Neurobiol 70:636–648.

Scott BH, Malone BJ, Semple MN (2007) Effect of behavioral context on representation of a spatial cue in core auditory cortex of awake macaques. J Neurosci 27:6489–6499.

Shadlen MN, Britten KH, Newsome WT, Movshon JA (1996) A computational analysis of the relationship between neuronal and behavioral responses to visual motion. J Neurosci 16:1486–1510.

Shannon RV, Zeng FG, Kamath V, Wygonski J, Ekelid M (1995) Speech recognition with primarily temporal cues. Science 270:303–304.

Singh NC, Theunissen FE (2003) Modulation spectra of natural sounds and ethological theories of auditory processing. J Acoust Soc Am 114:3394–3411.

Sivaramakrishnan S, Sterbing-D'Angelo SJ, Filipovic B, D'Angelo WR, Oliver DL, Kuwada S (2004) $GABA_A$ synapses shape neuronal responses to sound intensity in the inferior colliculus. J Neurosci 24:5031–5043.

Strickland EA, Viemeister NF (1997) The effects of frequency region and bandwidth on the temporal modulation transfer function. J Acoust Soc Am 102:1799–1810.

Suga N (2008) Role of corticofugal feedback in hearing. J Comp Physiol A Neuroethol Sens Neural Behav Physiol 194:169–183.

Ter-Mikaelian M, Sanes DH, Semple MN (2007) Transformation of temporal properties between auditory midbrain and cortex in the awake Mongolian gerbil. J Neurosci 27:6091–6102.

Thomas H, Tillein J, Heil P, Scheich H (1993) Functional organization of auditory cortex in the mongolian gerbil (*Meriones unguiculatus*). I. Electrophysiological mapping of frequency representation and distinction of fields. Eur J Neurosci 5:882–897.

Thornton SK, Semple MN, Sanes DH (1999) Conditioned enhancement and suppression in the developing auditory midbrain. Eur J Neurosci 11:1414–1420.

Victor J, Purpura K (1997) Metric-space analysis of spike trains: theory, algorithms and application. Netw Comp Neural Syst 8:127–164.

Viemeister NF (1979) Temporal modulation transfer functions based upon modulation thresholds. J Acoust Soc Am 66:1364–1380.

Wang L, Narayan R, Grana G, Shamir M, Sen K (2007) Cortical discrimination of complex natural stimuli: can single neurons match behavior? J Neurosci 27:582–589.

Wang X, Lu T, Snider RK, Liang L (2005) Sustained firing in auditory cortex evoked by preferred stimuli. Nature 435:341–346.

Wright BA, Zhang Y (2009) Insights into human auditory processing gained from perceptual learning. In: The cognitive neurosciences, Ed 4 (Gazzaniga MS, ed), pp. 353–366. Boston: MIT.

Zhang LI, Tan AY, Schreiner CE, Merzenich MM (2003) Topography and synaptic shaping of direction selectivity in primary auditory cortex. Nature 424:201–205.

Zohary E, Shadlen MN, Newsome WT (1994) Correlated neuronal discharge rate and its implications for psychophysical performance. Nature [Erratum (1994) 371:358] 370:140–143.

Zwicker E (1952) Die Grenzen der Hôrbarkeit der Amplitudenmodulation und der Frequenzmodulation eines Tones. Acustica Akust Beih 3.